
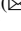





Nonlinear Inertia and Its Effect Within an X-shaped Mechanism

Zhengan Zhu  and Xingjian Jing  

Department of Mechanical Engineering, City University of Hong Kong, Hong Kong, China
xingjing@cityu.edu.hk

Abstract. This paper presents a new understanding and development related to nonlinear inertia and its effect in coupling with an X-shaped anti-vibration mechanism, which is validated by prototyping and experiments. The new inertial unit integrated in a well-designed X-shaped mechanism allows larger excitation displacements and more adjustable inertia ratios, resulting in significantly lower vibration transmissibility and resonance peak, and produces three different typical nonlinear inertia forms. A key parameter indicator (Ratio of Inertia) is proposed to identify and indicate the different types of nonlinearities, and the resulting beneficial effects are explored. The performance improvement in dynamics with respect to the linear counterpart is evaluated for different nonlinear inertia forms. The results show that: (a) The U-shaped symmetrical nonlinear inertia coupling with X-shaped mechanisms can provide better vibration isolation performance at low frequency; (b) High-frequency transmissibility can be tuned to different level, indicating a tunable band-suppress property, which is a unique property discovered in this study; (c) the nonlinear inertia contributes significantly to tune the interactive force between vibration source and object in the low frequency range (<10 Hz in our prototype) and obviously helpful and robust to stronger excitations. This study provides new insights into the application of nonlinear inertia in various engineering systems to achieve better passive vibration suppression or isolation.

Keywords: Passive vibration isolation · X-shaped mechanisms · Nonlinear inertia

1 Introduction

Vibration is a prevalent source of equipment degradation in engineering practice [1]. A common countermeasure is to implement isolators between the equipment and the vibration source, thereby reducing the vibration response [2]. The key to obtaining excellent vibration isolation performance is the selection of appropriate stiffness and damping. For this purpose, many novel control methods and structures have been proposed, including different passive and active methods and also those more recently developed for employing nonlinear benefits such as quasi-zero stiffness (QZS), high-static and low-dynamic stiffness (HSLDS), metamaterials, and X-shaped structure/mechanisms, etc. [3–7]. However, achieving satisfactory isolation performance at low frequency (e.g., below 5 Hz) and broad-band frequency remains a challenge for engineering practice [8].

Nonlinear vibration isolator solves the two contradictory points of the linear vibration isolator in enhancing the vibration isolation performance, that is, structural stability and low high-frequency transmissibility. Nonlinear isolators with high static and low dynamic stiffnesses and small resonant frequencies allow for a wide range of isolation frequencies while maintaining good stability [9, 10], which facilitates the design of isolators with low dynamic stiffness and high loading capacity. However, many passive stiffness adjustment methods suffer from modeling difficulties, poor stability and manufacturing accuracy. Especially for those materials with inherent nonlinearity, the control of nonlinear response and the selection of relevant design parameters will become more difficult without accurate models [4].

Bio-inspired X-shaped nonlinear vibration isolation systems have attracted a lot of interest recently. The X-shaped structure/mechanism has excellent nonlinear stiffness/damping and flexible tuning ability, which enables it to achieve ultra-low and broad-band frequency vibration suppression easily. In particular, the X-shaped vibration isolation system can lower the resonant frequency without sacrificing load capacity [8, 11, 12], decrease the resonant amplitude without worsening the high-frequency transmissibility [13, 14], and extend the frequency range for vibration isolation [1, 15]. Since Jing first proposed and studied the vibration isolation performance of X-shaped mechanism [4, 16], many researchers have conducted thorough studies on the nonlinear dynamic characteristics and vibration isolation performance of different kinds of X-shaped structures, such as symmetric/asymmetric X-shaped [10, 17], scissor-like platform [16, 18] and X-mount [19] et al. The work in [18] first introduced an inertial rotating unit into the X-shaped mechanism and shown that nonlinear inertia can significantly improve the vibration isolation performance at low and broad-band frequency.

It is important to note that, although there have been many efforts systematically analyzing the nonlinear vibration isolation performance of different types of X-shaped structures and thoroughly investigating the benefits of nonlinear stiffness and damping on vibration isolation systems with biological structure, there are still some critical points to be further investigated regarding the coupling of nonlinear inertia to X-shaped mechanisms, which are as follows. (1) What influence different types of nonlinear inertia can have on vibration suppression and structural stability; (2) What type of nonlinear inertia is more suitable for vibration control and what the influence it could bring in theory; and (3) how to exploit the benefits of nonlinear inertia more effectively through a reasonable arrangement of rotational units, etc. For the first two questions, previous studies have partially done in [9, 18] but still need to unveil more detailed understanding, and for the last one, the previous designs have resulted in nonlinear inertia that cannot be fully utilized due to limiting the range of motion in the vertical direction.

To address the issues above, this paper presents a totally new design of the inertial unit for mimicking a human swinging arm (as shown in Figs. 1 and 2). The new mechanism can offer more flexibility in tuning different leverage ratio such that larger excitation displacement can be allowed compared to the previous design, and the resulting nonlinear inertia characteristics of the rotational unit can be enhanced for different application scenario. Importantly, it is revealed that, (a) the new mechanism can offer more flexibility in tuning different structure parameters such that the resonant frequency and high-frequency transmissibility can be flexibly adjusted according to the practical

requirements, (b) the symmetrical shape (U-shaped) of the nonlinear inertia can provide better isolation performance and mass stability at low frequency, while two asymmetrical ones can have relatively better high-frequency transmissibility; (c) high-frequency transmissibility can be tuned to different level, indicating a tunable band-suppress property, which is a unique property discovered in this study; (d) since large excitation displacements are allowed, the nonlinear inertia can have stronger nonlinearity and larger inertia range, resulting in better vibration suppression performance. (e) a novel parametric indicator, Ratio of Inertia, is proposed to tune and identify different types of nonlinear inertia, which can exactly indicate the three benchmark nonlinear inertia types, and greatly facilitate the analysis and design.

The rest of the paper is organized as follows. The mathematical modelling of X-shaped isolation system is presented in Sect. 2. The nonlinear properties and its relationship with the structural parameters are analyzed in Sect. 3 and the effects of the parameters are summarized. The effects of different types of nonlinear inertia on vibration transmissibility and interactive forces are analyzed in Sect. 4. The nonlinear inertia and vibration isolation test of experimental prototype is conducted in Sect. 5 to verify the above theoretical results. A conclusion is drawn thereafter.

2 Modeling of the Novel Nonlinear Inertia Unit Coupling with an X-mechanism

The diagram of the proposed anti-vibration system is shown in Fig. 1 with detailed parametric notations.

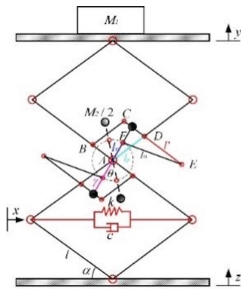


Fig. 1. Modeling of the anti-vibration system.

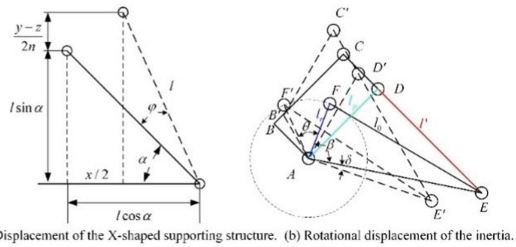


Fig. 2. The displacement due to relative motion.

The loading M_1 is supported by the X-shaped structure and the absolute displacements of the M_1 and the base are represented by y and z . l, l', l_r, l_0 and l_p are the rod length of the X-shaped structures and quadrilateral $ABCD$ is a parallelogram, as shown in Fig. 1. n, α, k and c are the number of layers, initial installation angle, horizontal stiffness and damping of the X-shaped structure, respectively.

As shown in Fig. 2, due to the relative motion between the displacement y and z , the deformation of the spring is x , the angle between the base and the rod changes by ϕ , and

the rotation angle of the inertial unit moving from the initial state AF to AF' is θ . The geometric relationship can be expressed as,

$$x = 2l \cos \alpha - 2\sqrt{l^2 - (l \sin \alpha + \hat{y}/2n)^2} \tag{1}$$

where, $\hat{y} = y - z$

$$\varphi = \arctan\left(\frac{l \sin \alpha + \hat{y}/2n}{l \cos \alpha - x/2}\right) - \alpha \tag{2}$$

$$\begin{cases} \beta = \arccos\left(\frac{l_r^2 + l_p^2 + l^2 + 2l_p l' \cos 2\alpha - l_0^2}{2l_r \sqrt{l_p^2 + l^2 + 2l_p l' \cos 2\alpha}}\right) \\ \delta = \arctan\left(\frac{l' - l_p}{l' + l_p} \tan(\alpha + \varphi)\right) - \arctan\left(\frac{l' - l_p}{l' + l_p} \tan \alpha\right) \end{cases} \tag{3}$$

$$\theta = \arccos\left(\frac{l_r^2 + l_p^2 + l^2 + 2l_p l' \cos 2(\alpha + \varphi) - l_0^2}{2l_r \sqrt{l_p^2 + l^2 + 2l_p l' \cos 2(\alpha + \varphi)}}\right) - \beta - \delta \tag{4}$$

According to the Lagrange principle, the motion equation of the anti-vibration system proposed in this paper can be obtained as,

$$\begin{aligned} (M_1 + \frac{1}{4}M_2)\ddot{y} + M_2\gamma^2\left(\frac{\partial\theta}{\partial\hat{y}}\right)^2\ddot{\hat{y}} + M_2\gamma^2\frac{\partial\theta}{\partial\hat{y}}\frac{\partial^2\theta}{\partial\hat{y}^2}\frac{\partial\hat{y}}{\partial y}\dot{z}^2 \\ + k(x - x_s)\frac{\partial x}{\partial\hat{y}}\frac{\partial\hat{y}}{\partial y} + (M_1 + M_2)g = -c\frac{\partial x}{\partial\hat{y}}\frac{\partial\hat{y}}{\partial t} \end{aligned} \tag{5}$$

For ease of calculation, the nonlinear terms in Eq. (5) are defined as f_1, f_2, f_3 and f_4 as $f_1(\hat{y}) = \gamma^2\left(\frac{\partial\theta}{\partial\hat{y}}\right)^2, f_2(\hat{y}) = \gamma^2\frac{\partial\theta}{\partial\hat{y}}\frac{\partial^2\theta}{\partial\hat{y}^2}\frac{\partial\hat{y}}{\partial y}, f_3(\hat{y}) = (x - x_s)\frac{\partial x}{\partial\hat{y}}\frac{\partial\hat{y}}{\partial y}$ and $f_4(\hat{y}) = \frac{\partial x}{\partial\hat{y}}$.

Then Eq. (5) can be simplified as,

$$\begin{aligned} (M_1 + \frac{1}{4}M_2 + M_2f_1(\hat{y}))\ddot{\hat{y}} + M_2f_2(\hat{y})\dot{\hat{y}}^2 + kf_3(\hat{y}) \\ + cf_4(\hat{y})\dot{\hat{y}} + (M_1 + M_2)g = -(M_1 + \frac{1}{4}M_2)\ddot{z} \end{aligned} \tag{6}$$

The detailed expressions of nonlinear functions f_1, f_2, f_3 and f_4 are all continuous $\hat{y} = 0$. These functions can be approximated by Taylor series as,

$$F_1 = \lambda_0 + \lambda_1\hat{y} + \lambda_2\hat{y}^2 + \lambda_3\hat{y}^3 \tag{7}$$

$$F_2 = \lambda_4 + \lambda_5\hat{y} + \lambda_6\hat{y}^2 + \lambda_7\hat{y}^3 \tag{8}$$

$$F_3 = \varepsilon_0 + \varepsilon_1\hat{y} + \varepsilon_2\hat{y}^2 + \varepsilon_3\hat{y}^3 \tag{9}$$

$$F_4 = \varepsilon_4 + \varepsilon_5\hat{y} + \varepsilon_6\hat{y}^2 + \varepsilon_7\hat{y}^3 \tag{10}$$

Therefore, replacing f_1, f_2, f_3, f_4 in Eq. (6) with F_1, F_2, F_3, F_4 , the equation of motion can be rewritten as,

$$\begin{aligned} (M_1 + \frac{1}{4}M_2 + M_2F_1(\hat{y}))\ddot{\hat{y}} + M_2F_2(\hat{y})\dot{\hat{y}}^2 \\ + kF_3(\hat{y}) + cF_4(\hat{y})\dot{\hat{y}} + (M_1 + M_2)g = -(M_1 + \frac{1}{4}M_2)\ddot{z} \end{aligned} \tag{11}$$

In Eq. (11), it can be seen that the unique nonlinear geometrical relationship of the anti-vibration system results in nonlinear equivalent mass $M_2F_1(\hat{y})$ and nonlinear inertia incurred conservation force $M_2F_2(\hat{y})\dot{\hat{y}}^2$, nonlinear stiffness $kF_3(\hat{y})$ and nonlinear damping term $cF_4(\hat{y})\dot{\hat{y}}$, which are all nonlinear functions of structural parameters.

3 Effect of Model Parameters on Nonlinear Characteristics

In this section, the influence of nonlinear inertial and the nonlinear inertial forces on the vibration isolation performance are investigated. To show the effect of model parameters on the nonlinear characteristics more intuitively, the displacement transmissibility is used to evaluate the vibration isolation performance, which is calculated by the harmonic balance method (HBM). The base excitation displacement and relative displacement can be set as $z = z_0 \cos(\omega t + \psi)$ and $\hat{y} = a \cos(\omega t)$. a, z_0, ω and ψ are the response amplitude, excitation amplitude, frequency and initial phase respectively. The displacement transmissibility T_d can be given by,

$$T_d = 20 \lg \left| \frac{\sqrt{a^2 + 2az_0 \cos \psi + z_0^2}}{z_0} \right| \tag{12}$$

Based on Eq. (12), the displacement transmissibility of the anti-vibration system can be calculated (Fig. 3). The amplitude of excitation displacement is 0.01 m, which ensures the validity of the Taylor series. The specific parameters can be found in [20].

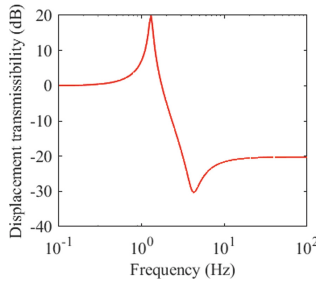


Fig. 3. The displacement transmissibility of the anti-vibration system.

From Fig. 3, it can be seen that the resonance frequency of the anti-vibration system is 1.3 Hz, which is less than the 1.5 Hz of the inertia-free system. The results indicate that the inertial unit affects the resonance frequency of the system. Moreover, the anti-resonance frequency of the system is 4.3 Hz, which means that it can achieve band-suppression isolation with a low cut-off frequency.

3.1 Effect of Length of Rods

The nonlinear inertia and nonlinear conservation force are $M_2F_1(\hat{y})$ and $M_2F_2(\hat{y})\dot{\hat{y}}^2$, which are mainly related to variables l_p, γ, l_r and l_0 . To evaluate the parametric effects

on those nonlinear terms and associated displacement transmissibility, a parametric influence analysis is conducted.

Assuming that other parameters remain unchanged, the rod length l_p , γ , l_r and l_0 change from 60 mm to 120 mm, 120 mm to 360 mm, 20 mm to 40mm and 170 mm to 200 mm, respectively. The three indicators including nonlinear inertia coefficient, nonlinear conversation force and displacement transmissibility are shown in Fig. 4.

From Fig. 4, the nonlinearity of inertia and nonlinear conversation force increase with the increase of the rod lengths l_p , γ and l_0 , and both exhibit asymmetrical properties. Contrary to rod lengths l_p , γ and l_0 , the nonlinearity of inertia and nonlinear conversation force increase with decreasing rod length l_r and exhibit two different forms of nonlinear curves, i.e., symmetrical and asymmetrical curves. When $l_r = 20$ mm, the nonlinear curve is U-shape, while the nonlinear curve shows asymmetric characteristic with rod lengths $l_r = 30$ mm and $l_r = 40$ mm.

For convenience of discussion, the asymmetrical inertia curves corresponding to the rod lengths l_p and l_0 are recorded as the high-compression-low-extension (HCLE) form and the low-compression-high-extension (LCHE) form, respectively, and the symmetrical nonlinear inertia curves corresponding to the rod length l_r are recorded as the high-compression-high-extension (HCHE) form. Regardless of the nonlinear inertia form, the resonance & anti-resonance frequency, peak value and slope, decrease with increasing nonlinearity. However, the high-frequency transmissibility increases with increasing nonlinearity.

3.2 Effect of the Mass Ratio η

To study the effect of mass on the nonlinearity, the mass ratio is defined as $\eta = M_2/M_1$. The ratio η is chosen from 0.03 to 0.30, and three indicators are shown in Fig. 5. The influence of η on the isolation performance shows similar trend to those of the rod length γ in Fig. 4.

3.3 Effect of the Angle α

The angle α of the X-shaped structure is selected between 40° and 50° . The effect of the angle α on the X-shaped supporting structure is shown in Fig. 6. The adjustment of angle α produces two typical nonlinear inertia forms and nonlinear conversation force, HCLE and LCHE. The HCLE nonlinearity contributes more to the reduction of the resonance and anti-resonance frequencies, while the LCHE nonlinearity can help to reduce the peaks slightly.

3.4 Effect of the Layers n

The layer number n is varying between 2 and 4, and the results are shown in Fig. 7. The change of layer number n has no effect on the nonlinearity type and the anti-resonance frequency but affects the value of the nonlinearity. The smaller the layer number n will produce more stronger nonlinearity, bigger resonant frequency but smaller peak value and anti-resonant peak, much shaper slope but higher high-frequency band-suppression level.

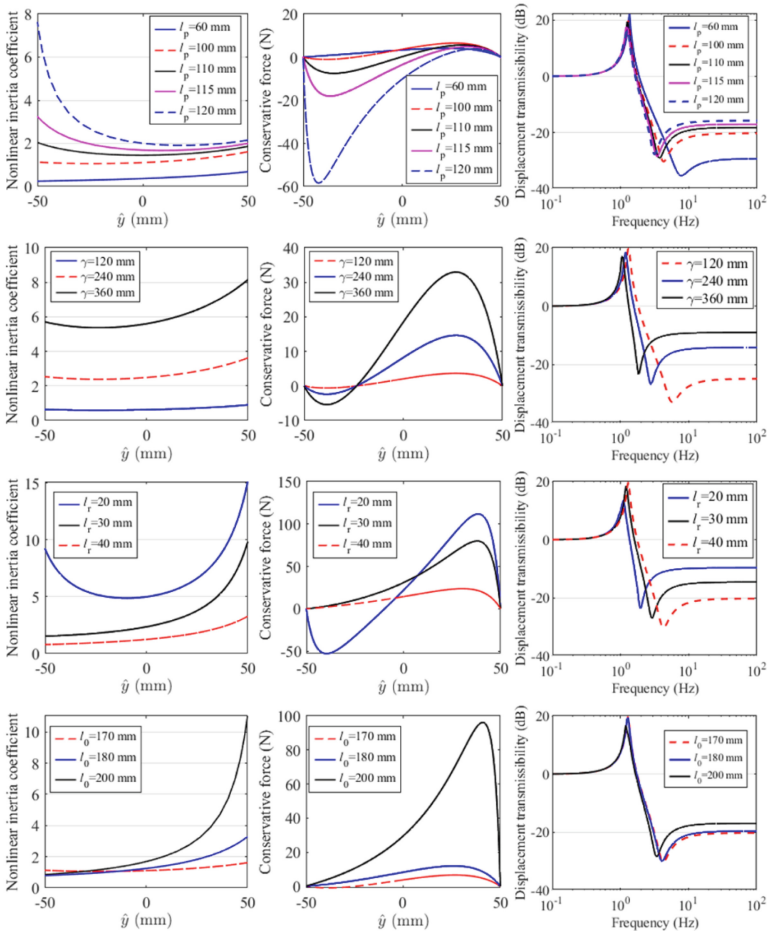


Fig. 4. The effect of different rod length.

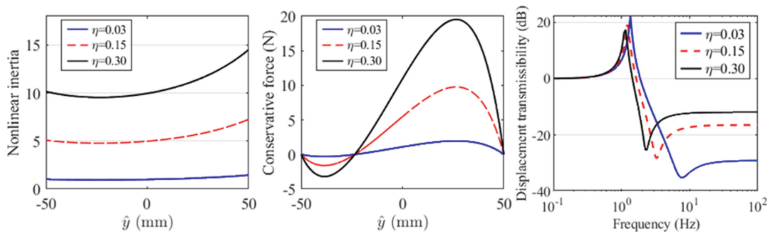


Fig. 5. The effect of the mass ratio η .

3.5 Unique Adjustable Vibration Suppression Properties

The desired beneficial nonlinearities for a given system must meet various practical requirements in design and implementation. The above parametric analysis shows that

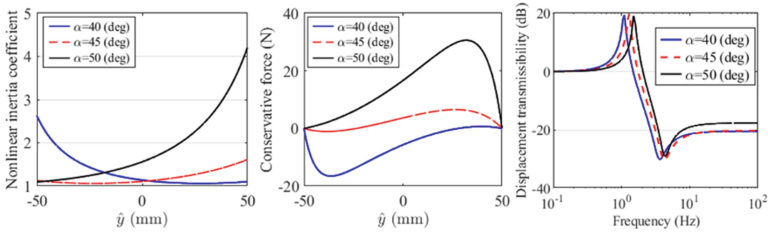


Fig. 6. The effect of the angle α .

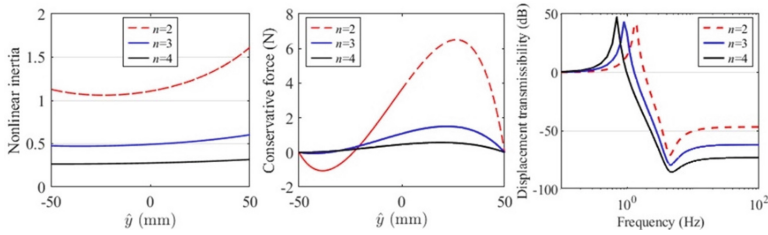
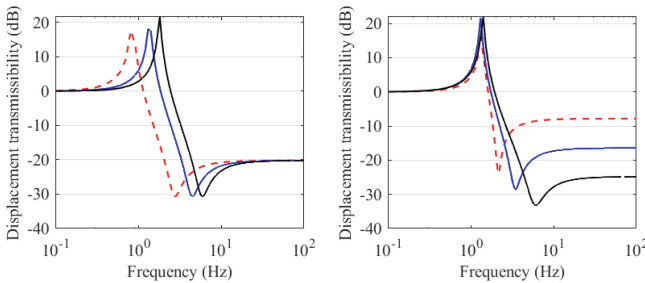


Fig. 7. The effect of the layers n .

the inertia parameters can affect the nonlinear properties and significantly lower the resonant frequency of the system. They can also adjust the high-frequency band-suppression transmissibility and slope, as shown in Fig. 8.



(a) Frequency with different parameters, (b) Transmissibility with different parameters.

Fig. 8. Design examples: Tunable resonant frequency and transmissibility

For Fig. 8(a), by decreasing the angle α , the rod length l_r , and the rod length γ , the resonance frequency is gradually reduced to below 1 Hz, while the high-frequency transmissibility and the decay slope remain constant. For Fig. 8 (b), by decreasing the angle α , rod length γ and increasing the rod length l_r , the high-frequency band-suppression transmissibility can be varied in different levels with unchanged resonant frequency and peak value. These results have never been disclosed before in the literature and demonstrate the very favorable nonlinear vibration isolation properties of the proposed mechanism in terms of adjustability, flexibility and effectiveness.

3.6 A Summary of Parametric Influence

In a summary, compared to traditional vibration isolation systems, some very interesting results can be further summarized as follows.

- (a) There are three typical forms of nonlinear inertia and nonlinear conservation forces, i.e., HCLE, LCHE and HCHE form, which have a significant effect on vibration transmissibility, i.e., reducing the resonance & anti-resonance frequency, peak value and slope.
- (b) For a given structural parameter setting of rod lengths of the inertia unit, the mass ratio can be easily adjusted to achieve different nonlinear characteristics, which is of great importance for engineering applications.
- (c) By adjusting the parameters, both the resonant frequency and the high-frequency transmissibility can be tuned to different levels without affecting each other, indicating a tunable resonance frequency and band-suppress property.

4 Understanding of Nonlinear Inertia-Related Forces

This section aims to further investigate the effects of different types of nonlinear inertia and their corresponding forces on vibration control and structural stability.

4.1 Influence on Transmissibility with Different Nonlinear Types

Define a rod length ratio (referred to as Ratio of Inertia (RoI)) as,

$$\zeta = l_0/l_r \quad (13)$$

where, l_0 and l_r are the rod lengths of the rotation unit, respectively. This ratio can work as a very critical factor to tune different nonlinear inertia types (i.e., HCLE, LCHE and HCHE) easily in the following studies. The nonlinear inertia coefficient, nonlinear conservation force and displacement transmissibility are shown in Fig. 9.

From the results, it can be summarized as follows.

By tuning the defined Ratio of Inertia ζ , the 3 typical nonlinear types of nonlinear inertia and nonlinear conservation forces can all be gradually obtained from the asymmetrical ones HCLE and LCHE to the symmetrical HCHE. The HCLE and LCHE nonlinearities can produce almost the same performance in vibration transmissibility. When the nonlinearities tend to be closer to the symmetrical nonlinearity HCHE, better vibration suppression can be achieved, but a little bigger of the high-frequency band-suppression level can be seen.

Robustness to Change of Excitation. To demonstrate the advantages of large excitation amplitudes, three typical nonlinear inertia curves ($\zeta = 6.20, 8.84, 7.10$) were selected, and the isolation performance under different excitation amplitudes was analyzed.

From the results in Fig. 10, it can be seen that,

- (a) A larger excitation results in better vibration isolation performance in all cases, i.e., smaller resonant & anti-resonant frequencies, smaller resonant peak values but the same high-frequency decay slope and anti-resonant peak value, and the same high-frequency band-suppression level.
- (b) The HCHE-type nonlinearity performs even better than other two when the excitation amplitude is increased with a much smaller resonant frequency and peak values.

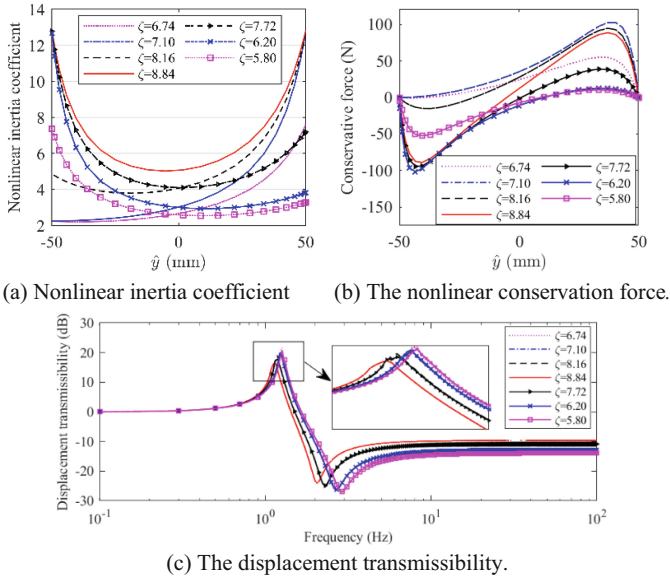


Fig. 9. The effect of different Ratio of Inertia ζ .

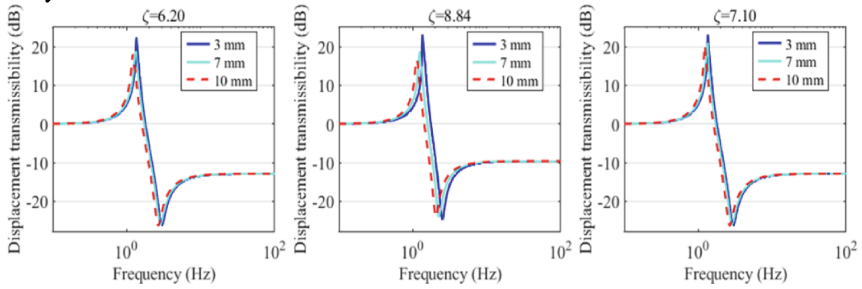


Fig. 10. Displacement transmissibility with different excitation amplitudes.

4.2 Influence on Interactive Force Around Equilibrium

The ideal situation in vibration control is that the interaction force between the vibration source and the protected object should always match the payload around the equilibrium. However, this interaction force will always vary around the equilibrium due to external vibration, causing the protected object to vibrate. Therefore, this interaction force can be a key indicator for evaluating the vibration control performance.

The payload mass, spring and damping coefficient of the linear isolation system moving on a 50 mm wave surface are 30 kg, 10 kN/m and 50 Ns/m, respectively. The spring force F_k , damping force F_c , nonlinear inertial force F_I , nonlinear inertia incurred conservative force F_e and combination of the forces with three typical nonlinear inertia forms are calculated under same input energy (0.5J) and shown in Fig. 11. The equivalent

interactive force for linear ($F_{L,E}$) and nonlinear system ($F_{NL,E}$) are as follows.

$$F_{L,E} = -k\hat{y} - c\dot{\hat{y}} \tag{14}$$

$$F_{NL,E} = -M_2F_1(\hat{y})\ddot{\hat{y}} - M_2F_2(\hat{y})\dot{\hat{y}}^2 - kF_3(\hat{y}) - (M_1 + M_2)g - cF_4(\hat{y})\dot{\hat{y}} \tag{15}$$

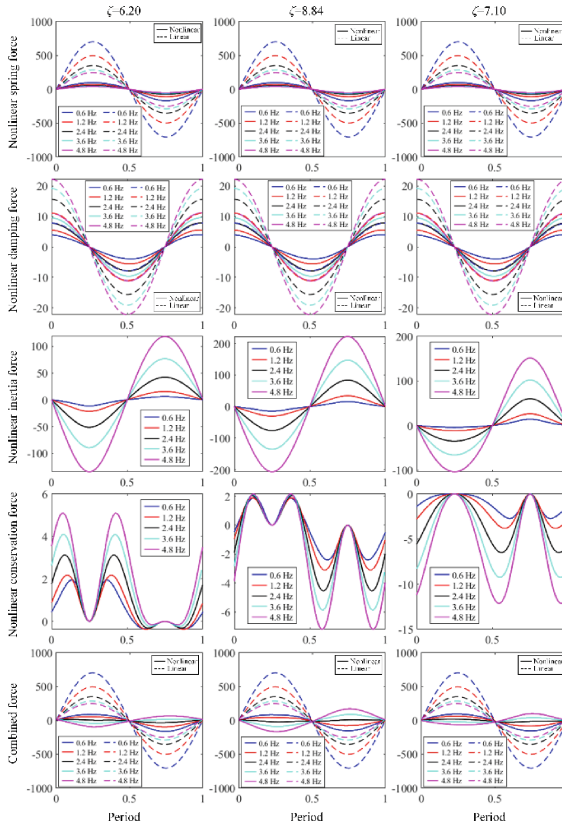


Fig. 11. Different forces with different frequencies in one cycle.

From Fig. 11, some interesting results can be summarized as follows:

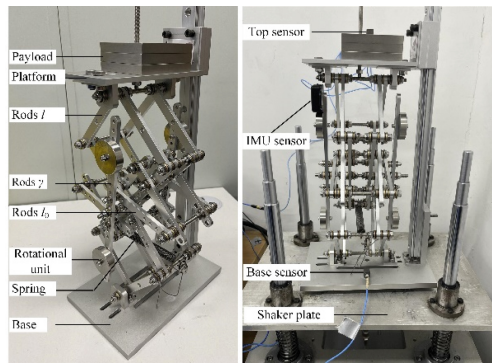
- (a) The fluctuations of nonlinear spring force and damping force all are significantly smaller than the linear system due to the dynamic coupling of the rotating unit.
- (b) As the excitation frequency increases, the linear/nonlinear damping force, nonlinear inertia force and inertia-incurred conservative force are all increased, while the linear/nonlinear stiffness forces are decreased.
- (c) Stiffness and nonlinear inertia forces are main factors in producing fluctuation of the interactive force and both are opposite to each other, which clearly shows that the nonlinear inertia force can be used to suppression vibration. The HCHE-type

nonlinear inertia can have much better function in balancing the interactive force both at extension and compression stages.

- (d) The inertia incurred conservative forces tend to be much smaller than the inertia forces, and tend to move the energy of the interactive force to high frequencies. This is another very good nonlinear feature for passive vibration isolation.

5 Prototyping and Experiments

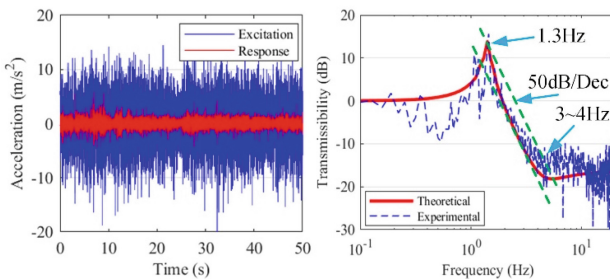
To further study and verify the effects of nonlinear inertia, a prototype of the proposed anti-vibration system will be fabricated and tested for in-depth understanding of the theoretical findings. The layout of the experimental prototype and the experimental setup are shown in Fig. 12, and the specific parameters can be found in [20].



(a) Layout of the prototype. (b) Experimental setup.

Fig. 12. The experimental prototype.

The frequency range of random excitation is selected from 0.5 Hz to 100 Hz, and the vibration response and transmissibility are shown in Fig. 13.



(a) The time series accelerate signals, (b) Transmissibility.

Fig. 13. The vibration response and transmissibility.

From Fig. 13, the resonance & anti-resonance frequency of the experimental prototype are 1.3 Hz and 4.3 Hz, respectively, which are consistent with the theoretical results.

Notably, the prototype achieves vibration suppression from around 1.9 Hz and reaches the anti-resonance peak at around 4 Hz with a very sharp decay ratio up to 50 dB/Dec, which exhibits excellent vibration suppression performance.

The analysis in Sect. 4.1 shows that nonlinear inertia types (HCLE, LCHE and HCHE) can be obtained by adjusting the Ratio of Inertia, and different types of nonlinear inertia will also produce different vibration isolation effects. To gain deeper understanding of the effect of nonlinear inertia on vibration isolation performance, it makes sense to test nonlinear inertia in experiments. The nonlinear inertia function can be written as $F_1(\hat{y}) = \gamma^2 \left(\frac{\partial \theta}{\partial \hat{y}} \right)^2$, and its shape depends mainly on the rotational angle θ and the relative displacement \hat{y} . Since the changes in the rotational angle θ relative to the relative displacement \hat{y} are difficult to measure, it is necessary to consider an easy-to-measure method. Nonlinear inertia function can be rewritten as,

$$\begin{aligned}
 F_1(\hat{y}) &= \gamma^2 \left(\lim_{\Delta \hat{y} \rightarrow 0} \left(\frac{\theta(\hat{y} + \Delta \hat{y}) - \theta(\Delta \hat{y})}{\Delta \hat{y}} \right) \right)^2 \\
 &= \gamma^2 \left(\lim_{\Delta t \rightarrow 0} \left(\frac{\theta(t + \Delta t) - \theta(t)}{\Delta t} \frac{\Delta t}{\hat{y}(t + \Delta t) - \hat{y}(t)} \right) \right)^2
 \end{aligned}
 \tag{16}$$

From Eq. (16), the nonlinear inertia can be obtained by measuring the angular velocity of the rotational unit and the relative motion velocity between the upper platform and the base. As shown in Fig. 12(b), an inertial measurement unit (IMU) sensor is placed on the rotating rod γ to measure the rotational angular velocity, and two acceleration sensors are placed on the upper platform and the base to measure the relative motion velocity. The nonlinear inertia coefficient under different Ratio of Inertia ζ is shown in Fig. 14.

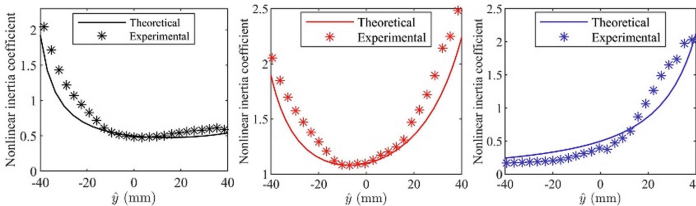


Fig. 14. Three typical nonlinear inertia.

From Fig. 14, the experimental and theoretical maximum errors of the three typical nonlinear inertias are 27.91%, 12.9% and 20.61%, respectively. This is caused by the assembly gap of the rotational unit and the non-vertical oscillation of the mechanism. However, the nonlinear inertia coefficients between experimental and theoretical have very similar changing trend for the testing range from -40 mm to $+40$ mm. Therefore, the errors caused by experimental tests are acceptable for verifying more the vibration isolation performance generated by different types of nonlinear inertia.

To demonstrate the effect of nonlinear inertia types on the vibration isolation performance, three typical nonlinear inertia forms (HCLE, HCHE, and LCHE) in Fig. 14

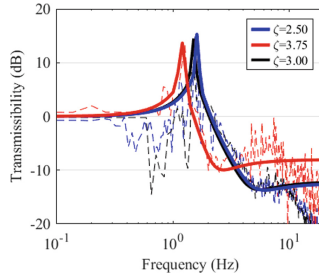


Fig. 15. The transmissibility of different Ratio of Inertia ζ .

were selected to calculate the transmissibility. The nonlinear inertia coefficients and transmissibility curves for Ratio of Inertia ζ are shown in Fig. 15.

From Fig. 15, the vibration transmissibility is almost the same for the asymmetrical nonlinearity HCLE and LCHE. As the nonlinearities tend to be closer to the symmetrical nonlinearity HCHE, better vibration suppression can be achieved, i.e., smaller resonance & anti-resonance frequency and peak values, and sharper decay rate, but a little bigger of the high-frequency band-suppression level. That is consistent with the theoretical analysis in Sect. 4.

6 Conclusion

This study is to reveal what nonlinear inertia there could be, how they are related to parametric change, and what influence they have. To this aim, a nonlinear inertia unit specially designed and intentionally embedded in an X-shaped mechanism is investigated for achieving more adjustability of nonlinear properties and revealing more in-depth nonlinear influence incurred by the inertial unit coupling with a nonlinear stiffness-damping system produced by the X-shaped mechanism. Based on theoretical analysis and experimental test, it is revealed that,

- (a) There are 3 typical nonlinear inertia incurred nonlinear forces (including nonlinear inertia and nonlinear conservation force) referred to as HCLE, LCHE and HCHE-types under different parameters producing different influences.
- (b) The symmetric nonlinear form HCHE can produce more reduction in resonance & anti-resonance frequency and peak value; while two asymmetrical ones can have relatively better transmissibility at high frequency;
- (c) High-frequency transmissibility can be tuned to different level, indicating a tunable band-suppress property.
- (d) Larger excitation results in better vibration isolation performance in all cases.
- (e) A unique test method is proposed to measure the nonlinear inertia of the prototype, which can provide a reference for similar research.

The studies not only reveal what and how nonlinear inertia contribute to vibration isolation but also provide totally new knowledge, unique understanding and novel associated analysis methods on exploiting nonlinear influence in engineering systems, and thus

will definitely bring benefits to a broad spectrum of academic studies and engineering practices related to nonlinear dynamics and vibration control.

Acknowledgement. The authors acknowledge the financial support from a CityU Strategic Research Grant (7005925), a startup fund of City University of Hong Kong (Grant No.9380140), a General Research Fund (11202323) of Hong Kong RGC, and a CityU Applied Research Grant (9667258).

References

1. Liu, C., Jing, X., Daley, S., Li, F.: Recent advances in micro-vibration isolation. *Mech. Syst. Signal Process.* **56–57**, 55–80 (2015)
2. Leng, D., Zhu, Z., Liu, G., Li, Y.: Neuro fuzzy logic control of magnetorheological elastomer isolation system for vibration mitigation of offshore jacket platforms. *Ocean Eng.* **253**, 111293 (2022)
3. Leng, D., Feng, W., Ning, D., Liu, G.: Analysis and design of a semi-active X-structured vibration isolator with magnetorheological elastomers. *Mech. Syst. Signal Process.* **181**, 109492 (2022)
4. Jing, X.: The X-structure/mechanism approach to beneficial nonlinear design in engineering. *Appl. Math. Mech.* **43**, 979–1000 (2022)
5. Chen, S., et al.: Design and experiment of dual micro-vibration isolation system for optical satellite flywheel. *Int. J. Mech. Sci.* **179**, 105592 (2020)
6. Zhang, M., Jing, X.: Switching logic-based saturated tracking control for active suspension systems based on disturbance observer and bioinspired X-dynamics. *Mech. Syst. Signal Process.* **155**, 107611 (2021)
7. Ning, D., Sun, S., Li, H., Du, H., Li, W.: Active control of an innovative seat suspension system with acceleration measurement based friction estimation. *J. Sound Vib.* **384**, 28–44 (2016)
8. Kamesh, D., Pandiyan, R., Ghosal, A.: Passive vibration isolation of reaction wheel disturbances using a low frequency flexible space platform. *J. Sound Vib.* **331**, 1310–1330 (2012)
9. Feng, X., Jing, X., Xu, Z., Guo, Y.: Bio-inspired anti-vibration with nonlinear inertia coupling. *Mech. Syst. Signal Process.* **124**, 562–595 (2019)
10. Chai, Y., Jing, X., Chao, X.: X-shaped mechanism based enhanced tunable QZS property for passive vibration isolation. *Int. J. Mech. Sci.* **218**, 107077 (2022)
11. Yan, B., Ma, H., Zhang, L., Zheng, W., Wang, K., Wu, C.: A bistable vibration isolator with nonlinear electromagnetic shunt damping. *Mech. Syst. Signal Process.* **136**, 106504 (2020)
12. Yan, B., Ma, H., Yu, N., Zhang, L., Wu, C.: Theoretical modeling and experimental analysis of nonlinear electromagnetic shunt damping. *J. Sound Vib.* **471**, 115184 (2020)
13. Jing, X.J., Lang, Z.Q., Billings, S.A.: Nonlinear influence in the frequency domain: alternating series. *Syst. Control Lett.* **60**, 295–309 (2011)
14. Jing, X.J., Lang, Z.Q.: Frequency domain analysis of a dimensionless cubic nonlinear damping system subject to harmonic input. *Nonlinear Dyn.* **58**, 469–485 (2009)
15. Jing, X.J., Lang, Z.Q., Billings, S.A., Tomlinson, G.R.: Frequency domain analysis for suppression of output vibration from periodic disturbance using nonlinearities. *J. Sound Vib.* **314**, 536–557 (2008)
16. Sun, X.J., Jing, X.: Analysis and design of a nonlinear stiffness and damping system with a scissor-like structure. *Mech. Syst. Signal Process.* **66**, 723–742 (2016)

17. Wang, Y., Jing, X.: Nonlinear stiffness and dynamical response characteristics of an asymmetric X-shaped structure. *Mech. Syst. Signal Process.* **125**, 142–169 (2019)
18. Feng, X., Jing, X.: Human body inspired vibration isolation: beneficial nonlinear stiffness, nonlinear damping & nonlinear inertia. *Mech. Syst. Signal Process.* **117**, 786–812 (2019)
19. Bian, J., Jing, X.: Analysis and design of a novel and compact X-structured vibration isolation mount (X-Mount) with wider quasi-zero-stiffness range. *Nonlinear Dyn.* **101**, 2195–2222 (2020)
20. Zhu, Z., Wang, Y., Wang, Y., Jing, X.: Nonlinear inertia and its effect within an X-shaped mechanism – Part I: Modelling & nonlinear properties. *Mech. Syst. Signal Process.* **200**, 110590 (2023)